Coiling, Entrainment, and Hydrodynamic Coupling of Decelerated Fluid Jets

Christopher Dombrowski,[1] Braddon Lewellyn,[1] Adriana I. Pesci,[1]
Juan M. Restrepo,[1,2,3] John O. Kessler[1] and Raymond E. Goldstein[1,2]
[1]*Department of Physics,* [2]*Program in Applied Mathematics,*
and [3]*Department of Mathematics, University of Arizona, Tucson, AZ 85721*
(Dated: December 13, 2004)

From algal suspensions to magma upwellings one finds jets which exhibit complex symmetry-breaking instabilities as they are decelerated by their surroundings. We consider here a model system – a saline jet descending through a salinity gradient – which produces dynamics unlike those of standard momentum jets or plumes. The jet coils like a corkscrew within a conduit of viscously entrained fluid, whose upward recirculation braids the jet, and nearly confines mixing to the narrow conduit. We show that the underlying jet structure and certain scaling relations follow from similarity solutions to the fluid equations and the physics of Kelvin-Helmholtz instabilities.

PACS numbers: 47.20.-k, 92.10.-c, 95.30.Lz, 47.54.+r

The broad range of physical and biological systems which exhibit fluid jets and plumes often display symmetry-breaking instabilities as the injected fluid interacts viscously with its surroundings. Examples include helical jets outflowing from a galactic nucleus [1], upwelling magma conduits [2], plumes from hydrothermal vents [3], and filamentary downwellings in algal suspensions [4]. Key issues in all are mixing and entrainment by the jet and the nonlinear regime far beyond the instabilities. Here we study a jet, which unlike momentum jets (e.g. the Bickley jet [5]), has a different density than the surrounding fluid, which in turn is stratified. Specifically, we study a fluid jet that decelerates by descent through a linear density gradient, differing from the surround only by the concentration of the solute that defines the gradient. This system operates at modest Reynolds numbers, quite distinct from turbulent plumes such as smoke stacks, effluent discharges, and volcanic eruptions [6]. In our system, the dynamics of single jets and pairs derive from a complex flow field created as they penetrate the gradient (Fig. 1), organized around a *conduit* of entrained fluid [2, 7, 8] braiding the jet, supporting wavelike or singular excitations on its wall [9]. We show that the coiling instability is a bifurcation which can be understood through similarity solutions of the fluid equations and the physics of Kelvin-Helmholtz instabilities. Like coordinated flapping of nearby filaments in a flowing soap film [10] which depends strongly on their separation, we also find coupled, synchronized coiling which varies with the separation of nearby jets.

An experimental control parameter is the flux Q of the pump driving the flow, or the average velocity $u = Q/\pi a^2$ of the fluid exiting the nozzle of radius a. Over the range studied $0.02 \leq Q \leq 5$ cm^3/hr ($0.15 \leq u \leq 40$ cm/s) and with $\nu = 0.01$ cm^2/s the kinematic viscosity of water, the jet Reynolds number is $Re = ua/\nu \sim 0.4 - 100$, well in the laminar regime. The diffusion constant of salt $D = 1.5 \times 10^{-5}$ cm^2/s gives a Schmidt number $Sc = \nu/D \sim 10^3$; mechanical dissipation dominates diffusion, and the Peclet number $Pe = Re \times Sc$ is very large, so advection also dominates diffusion. This latter aspect, the stratification, and finite Reynolds number effects together make this problem unlike pure momentum jets or diffusive plumes. A jet introduced into the fluid produces a steady conduit in $5 - 10$ s, as entrained flow builds around the jet through vorticity diffusion. The conduit edge, clearly seen in Fig. 1, has a width $\lesssim 0.01$ cm. The jet, inside the conduit, remains straight until the velocity exceeds a critical value u^*, beyond which it

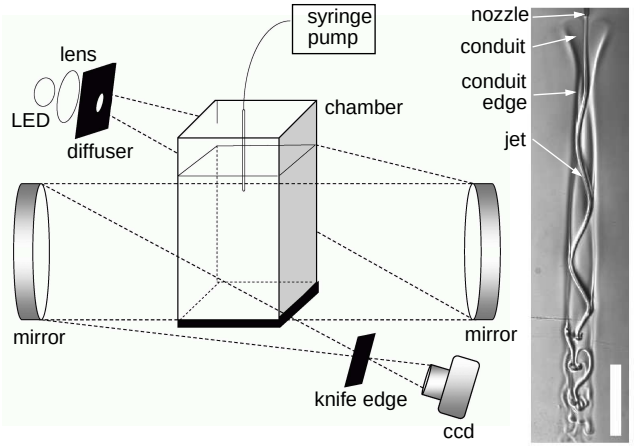

FIG. 1: Left; each half of the stereoscopic Schlieren system has 6" F/10 parabolic mirrors, LED illumination, and a knife-edge at the focus. 12-bit digital CCD cameras (Hamamatsu C7300) with $80-200$mm f/2.8 lenses acquire images to a PC. The chamber is a parallelipiped $18 \times 18 \times 61$ cm of 6mm plate glass. Jets exit a nozzle of radius $a = 0.025$ cm attached to a syringe pump (New Era Pump Systems N1000). Salinity gradients were produced by the "two-bucket" method, measured in situ by suspending 5 mm floats (American Density Materials). Particle Imaging Velocimetry was performed with a He-Ne laser sheet, suspended microspheres (Sphericel, Potters Ind., $\rho = 1.1$ g/cm^3, mean diameter 11.7μm) and software analysis (Dantec). Right; flow features, with 5 mm scale.

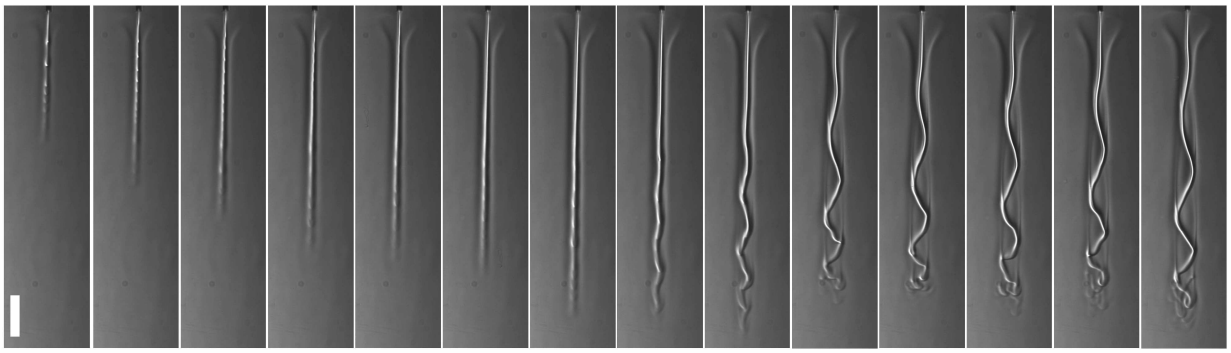

FIG. 2: Coiling instability. With increasing velocity the jet penetrates further into the gradient and then coils. Bar is 5 mm.

becomes helical (Fig. 2). The conduit hugs a straight jet tightly beyond ~ 5 mm below the nozzle, but flares out closer. When coiling begins the conduit widens so the jet is inscribed on it, like the buckling of constrained elastica [11]. The frequency f, wavelength λ and wave speed c are finite at u^*, increasing slowly beyond (Figs. 3c & d).

Consider first the regime $u < u^*$, and the *termination length* z^*, the distance between the injector and location at which image analysis can no longer differentiate the jet from its surroundings. Even when the jet density exceeds that of the surroundings at the chamber bottom, z^* is much less than the overall fluid depth H, so diffusional spreading of the jet clearly diminishes its density as it descends. Apart from an offset at small u, Fig. 3a shows that, $z^* \sim u^{1/2}$, and apart from a transition zone very near the nozzle, the jet width collapses onto a common *line* versus z/z^* (Fig. 3b). To explain these results, consider an incompressible axisymmetric flow $\mathbf{u}(r,z) = u(r,z)\hat{\mathbf{z}} + v(r,z)\hat{\mathbf{r}}$ and salt concentration $S(r,z)$. For a slender jet, the leading terms in the Navier-Stokes and advection-diffusion equations are [12, 13]

$$u\frac{\partial u}{\partial z} + v\frac{\partial u}{\partial r} = \nu\frac{1}{r}\frac{\partial}{\partial r}\left(\frac{r\partial u}{\partial r}\right) + g\kappa S \qquad (1)$$

$$u\frac{\partial S}{\partial z} + v\frac{\partial S}{\partial r} = D\frac{1}{r}\frac{\partial}{\partial r}\left(\frac{r\partial S}{\partial r}\right) , \qquad (2)$$

where the constant κ relates salinity and density changes. Far from the jet, the salinity asymptotes to the gradient: $\lim_{r\to\infty} S(r,z) = S_0 + S_G z/H$. The existence of the *stratification length* $\ell_G = (S_G/S_j)H$ eliminates the possibility that (1) and (2) possess a strict similarity solution. Since $\ell_G \gg z^*$, we explore the notion of a *local similarity* solution to (1) and (2) in the absence of a gradient. Computing the velocity from a stream function, $u = (1/r)\partial\psi/\partial r$ and $v = -(1/r)\partial\psi/\partial z$, we propose

$$\psi = \nu z^\alpha f(\xi) , \qquad S = \frac{\nu^2}{g}d^4 z^\delta \phi(\xi) , \qquad \xi = d\frac{r}{z^\beta} . \quad (3)$$

The dimensionless factor d is found below. Eqs. (1) and (2) reduce to ODEs if $\alpha = 1$ and $\delta = \alpha - 4\beta$. Unlike free diffusion [12, 13], here, as in the Bickley jet [5], the nozzle is a source of momentum, whose conservation constrains the exponents. For the momentum flux $M \sim \int dr r u^2 \sim z^{2(\alpha-\beta)}\int d\xi (f'^2/\xi)$ to be conserved the z-dependence must vanish, yielding $\beta = 1$, $\delta = -3$.

Define the edge of the jet by the radius r_j at which S is some fraction of its centerline value, hence at some $\xi = \tilde{\xi}$. With $\beta = 1$ the edge is the straight line $r_j = (\tilde{\xi}/d)z$, like the data of Fig. 3b, but the role of z^* in collapsing the data is not yet shown. We can find d by noting [13] that if at some z_0 we know the flux Q and integrated salt concentration C, then the similarity solutions yield $Q = 2\pi\nu z_0 f(\infty)$ and $C = 2\pi d^4(\nu^2/g z_0)\int d\xi\xi\phi$. Hence, $d \sim Q^{1/2}(\Delta\rho_j)^{1/2}$, where $\Delta\rho_j$ is the density difference between the jet and pure water. We hypothesize that z^* can be found from the difference ΔS between the falling salinity at the jet centerline, computed from the similarity solution, and the rising salinity of the background,

$$\Delta S \sim \frac{\nu^2 d^4 \phi(0)}{g z^3} - S_G\frac{z}{H} . \qquad (4)$$

When $\Delta S = 0$ the descending jet terminates at $z^* \sim d \sim Q^{1/2}(\Delta\rho_j)^{1/2}$, the dependence on Q (hence on u) being in agreement with data in Fig. 3a. The half-width of the jet thus obeys a scaling form, $r_j \sim z/z^*$ independent of the flux Q, consistent with the data (Fig. 3b).

The coiling instability exhibits a scaling law for the buckling velocity $u^*/G \sim (\Delta\rho_j)^{-\gamma}$, with $\gamma \sim 1.5$ (Fig. 4a), where G is the dimensionless maximum salinity in the gradient, S_G, measured in M/l. We find that an explanation for this centers around the flow field in the conduit. PIV analysis (Fig. 5a) reveals that there is a strong return flow within the conduit and very small flow beyond it. A simple model of this involves *three* fluids: a jet of radius a, density ρ_j, a conduit of radius b with pure water, within a surround of density ρ_s in a cylindrical tank of radius R. Assuming near-parallelism of the flow and solving $\nabla^2 u_i(r) = K_i$, with $K_i = (\partial p_i/\partial z + \rho_i g)/\eta$ in each domain, with continuity in velocity and viscous stress at the two interfaces we obtain the full flow field.

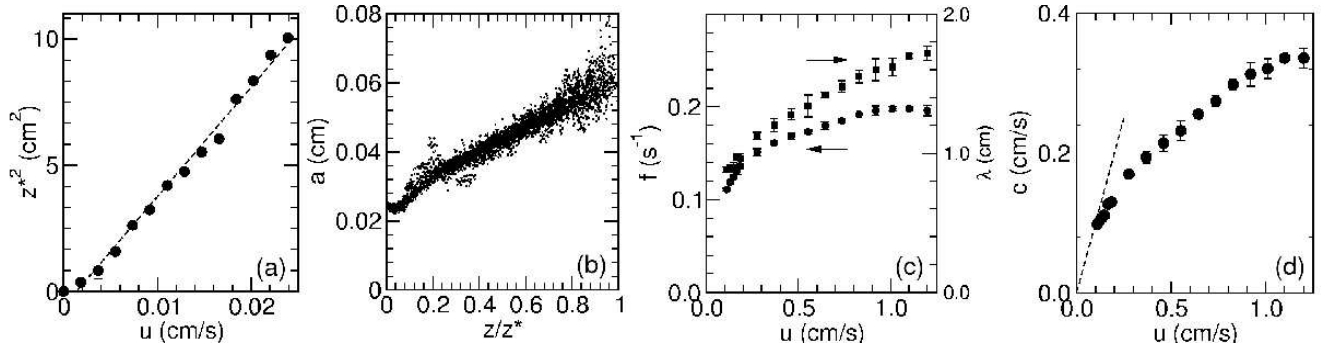

FIG. 3: Jet data. (a) square of the termination length z^* versus nozzle velocity, showing linear relationship, (b) jet width as a function of z/z^*. Oscillations near $z/z^* \sim 1$ show emergence of an axisymmetric instability; deviations at small z/z^* reflect the influence of the flaring conduit. Coiling frequency and wavelength (c) and wave speed (d) as functions of jet velocity. In (d), dashed line is the identity expected from the Kelvin-Helmholtz physics, which is accurately obeyed at onset.

For a given jet radius a and parameters $\{K_i\}$, the conduit radius b follows from mass conservation. Using representative parameters, Fig. 4b shows the very strong velocity gradient within the conduit and the clear return flow along the outer edge. The relative smallness of the velocity at the conduit edge implies that this geometry is akin to two-phase pipe flow with a no-slip boundary condition at the wall: the "core-annular" flow of lubricated pipelines [14], the inner jet playing the role of the oil, the outer fluid, the water. Stability analysis for that flow shows that when $b \gtrsim 1.2a$ the most unstable mode is helical with wavelength $\lambda \sim 7.5b$ [15], and the axisymmetric mode is also unstable. That $\lambda \sim b$ is expected, since the width of the shear layer sets the scale of the unstable mode [16]. Although this coiling is superficially similar to that of a viscous jet impinging on a surface [17, 18], it is distinguished by the role of shear.

We propose that the coiling instability occurs when the advected vertical momentum flux balances the radial flux, $u^2/\lambda \sim v^2/a$. The similarity solution yields $v/u \sim d \sim (\Delta\rho_j Q)^{1/2}$, and the three-fluid model shows that when the outer fluid is in hydrostatic equilibrium ($K_s = 0$), and the container is large ($R/a \gg 1$), then $b/a \simeq [(\rho_j - \rho_s)/(\rho_s - \rho_c)]^{1/2}$. Evaluating this at $z = z^*$ and using $\lambda \sim b$ we find $Q^* \sim (\Delta\rho_j)^{-3/2}$, in agreement with the results in Fig. 3e. In shear-driven instabilities the wave speed c is generally the velocity at the junction between the two opposing flows. Identifying that point with the edge of the jet, Fig. 4b shows that the velocity there is just slightly less than the average velocity u in the jet. The data in Fig. 3d show that c is indeed very nearly equal to u near the instability onset, deviating downward at much higher velocities. This would appear to follow from the ever larger backflow in the conduit.

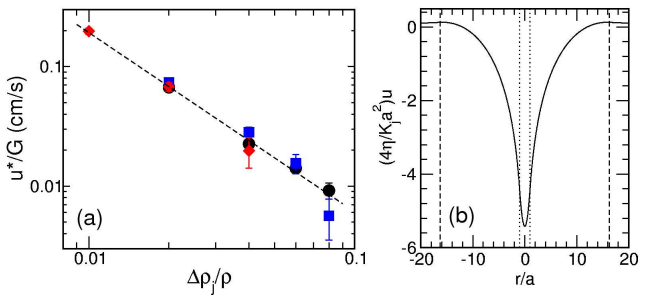

FIG. 4: (a) Critical buckling velocity as a function of the relative density offset of the jet, rescaled by dimensionless gradient: $G = 2$ (black circles), $G = 1$ (blue squares), and $G = 0.5$ (red diamonds). (b) Velocity profile in 3-fluid model, with jet (dotted) and conduit (dashed) locations shown.

Using suspended microspheres we obtained both streak images and vorticity (from PIV analysis) of a coiled jet. The streak image in Fig. 5b shows that the jet is *braided by a helical vortex*; when visualized in cross section, regions of clockwise and counterclockwise circulation appear to alternate down the jet (Fig. 5c), analogous to flows proposed in the serpentine instability of two-dimensional plumes [19]. The circulation within the conduit – down along the jet, up at the conduit edge – is shown by the vorticity in Fig. 5a, obtained by averaging over several periods of coiling, consistent with the three-fluid model profile in Fig. 4. The coupling between nearby jets expected from this vorticity was studied with an apparatus which holds two nozzles parallel at a variable centerline separation s, each fed from a syringe pump. If nearly touching, the two jets share a single conduit, appearing almost as one from the front (5c) or side (5d). If further apart, yet closer than a conduit diameter, the dynamics (not shown) is rather complex, even chaotic. Once the separation exceeds a conduit diameter, there is striking synchronization of phase; from the front (5e), the jets are mirror images, while from the side (5f) they are perfectly aligned. Beyond a critical separation s^* which varies with velocity ($s^* \sim 10$mm for $u \sim 5$ mm/s), the jets instead are *nested* (5g), and exhibit slow oscillations in the width of their conduits.

We suggest these complex coupled dynamics arises

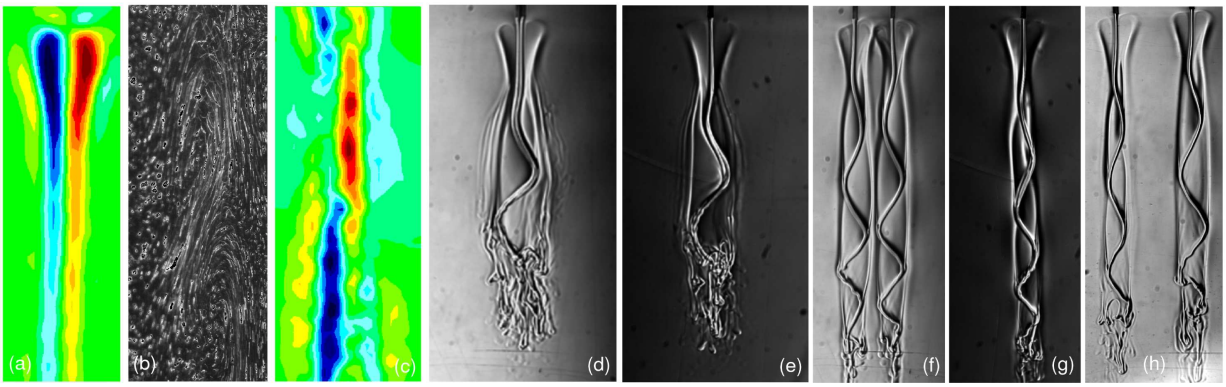

FIG. 5: Flow imaging and measurement. (a) vorticity from PIV near nozzle, averaged over many coiling periods, showing opposite senses of recirculation on either side of jet. (b) Streak image of suspended microspheres in the strongly coiled regime, (c) vorticity map in coiled regime, about one half-period shifted from (b). (d) & (e) front and side views of two separate jets which have merged inside a shared conduit; front (f) and side (g) views of two nearby jets which synchronize as mirror images, and front view of distant nested jets (h).

from competing viscous and inertial effects. Studies of the dynamics of elastic sheets with sinusoidal traveling-wave deformations [20] and rotating rigid helices [21, 22] show that the rate of viscous dissipation is greatly reduced in nested configurations, reflecting the smaller velocity gradients in such an arrangement. Although minimization of dissipation is not, in general, a mechanical driving force, it might explain that why at least at large separations the jets arrange themselves to be nested (Fig. 5h). It would not appear to explain why the two jets adopt mirror-image configurations when close. A possible explanation for the latter stems from the fact that the Reynolds number in this regime is on the order of unity, so inertial effects may compete with dissipation. When the jets are precisely out of phase, as in Fig. 5f, the fluid in the regions of closest approach of the jets flows rapidly, reducing the pressure there through the Bernoulli effect, possibly driving the jets together. A detailed theory of these effects remains an open problem.

The complex flow fields shown here arise from remarkably simple ingredients – a saline fluid jet descending into density-stratified surroundings – which produce a conduit with counter-propagating shear flow, dynamical instabilities, and coupling between nearby jets. The dynamics neither conforms exclusively to standard momentum jet or plume conceptualizations. With small modifications this experiment can include baroclinic effects, providing a simple model to address mixing in oceanic flows, such as gravity currents along undersea canyons [23].

We thank J.W. Beck, R. Daly, L. Mahadevan, K. Visscher, and W.R. Young for discussions. This work was supported by NSF CTS0079725 and PHY0219411.

[1] A. P. Lobanov and J. A. Zensus, Science **294**, 128 (2001).
[2] J. A. Whitehead and K. R. Helfrich, Nature **336**, 59 (1988).
[3] P. A. Rona, K. G. Bemis, D. Silver, and C. D. Jones, Marine Geophys. Res. **23**, 147 (2002).
[4] J. O. Kessler, Nature **313**, 218 (1985).
[5] P. G. Drazin and W. H. Reid, *Hydrodynamic Stability* (Cambridge University Press, Cambridge, 1981).
[6] J. S. Turner, *Buoyancy Effects in Fluids* (Cambridge University Press, Cambridge, 1973).
[7] K. Helfrich and J. Whitehead, Geophys. Astrophs. Fluid Dyn. **51**, 35 (1990).
[8] A. R. Tenner and B. Gebhart, Int. J. Heat Mass Transfer **14**, 2051 (1971).
[9] A. I. Pesci, M. A. Porter, and R. E. Goldstein, Phys. Rev. E **68**, 056405 (2003).
[10] J. Zhang, S. Childress, A. Libchaber, and M. Shelley, Nature **408**, 835 (2000).
[11] G. Domokos, P. Holmes, and B. Royce, J. Nonlin. Sci. **7**, 281 (1997).
[12] T. Fujii, Int. J. Heat Mass Transfer **6**, 597 (1963).
[13] R. S. Brand and F. J. Lahey, J. Fluid Mech. **29**, 305 (1967).
[14] D. D. Joseph, R. Bai, K. P. Chen, and Y. Y. Renardy, Annu. Rev. Fluid Mech. **29**, 65 (1997).
[15] H. H. Hu and N. Patankar, J. Fluid Mech. **290**, 213 (1995).
[16] T. E. Faber, *Fluid Dynamics for Physicists* (Cambridge University Press, Cambridge, 1995).
[17] G. I. Taylor, Proc. 12th Intl. Congr. Appl. Mech., Stanford p. 382 (1968).
[18] L. Mahadevan, W. S. Ryu, and A. D. T. Samuel, Nature **392**, 140 (1998).
[19] J. R. Lister, J. Fluid Mech. **175**, 413 (1987).
[20] G. Taylor, Proc. Roy. Soc. London A **209**, 447 (1951).
[21] M. Kim et al., Proc. Natl. Acad. Sci. (USA) **100**, 15481 (2003).
[22] M. Kim and T. R. Powers, Phys. Rev. E **69**, 061910 (2004).
[23] R. H. Kase, J. B. Girton, and T. B. Sanford, J. Geophys. Res. **108**, 3181 (2003).